Full title:

A planar neuromuscular controller to simulate age-related adaptation strategies in the sit-to-walk movement.

Short title:

A planar neuromuscular controller for the sit-to-walk movement

Eline van der Kruk*[1] & Thomas Geijtenbeek[1,2]

[1]Department of Biomechanical Engineering, Faculty of Mechanical Engineering (3me), Delft University of Technology, the Netherlands

[2] Goatstream, Utrecht, the Netherlands

*corresponding author: e.vanderkruk@tudelft.nl

Abstract

Standing up from a chair is a key daily life activity that is sensitive to functional limitations as we age and therefore associated with falls, frailty, and institutional living. Predictive neuromusculoskeletal models can potentially shed light on the interconnectivity and interdependency of age-related changes in neuromuscular capacity, reinforcement schemes, sensory integration, and adaptation strategies during stand up. Most stand-up movements transfer directly into walking (sit-to-walk). The aim of this study was to develop and validate a neuromusculoskeletal model with reflex-based muscle control that enables simulation of the sit-to-walk movement, under various conditions (seat height, foot placement), reduced muscular capacity, reduced neural capacity, and altered movement objectives. We developed a planar sit-to-walk musculoskeletal model (11 degrees-of-freedom, 20 muscles) and neuromuscular controller, consisting of a two-phase stand-up controller and a reflex-based gait controller. The stand-up controller contains generic neural pathways of delayed proprioceptive feedback from muscle length, force, velocity, and upper-body orientation (vestibular feedback) and includes both monosynaptic an antagonistic feedback pathways. The control parameters where optimized using a shooting-based optimization method. Simulations were compared to recorded kinematics, ground reaction forces, and muscle activation from young and older adults. The simulated kinematics closely resemble the measured kinematics and muscle activations, and the adaptation strategies, that resulted from alterations in seat height, are comparable to those observed in adults. The simulation framework and model are publicly available.

Keyword: sit-to-stand, sit-to-walk, ageing, stand up, neuromuscular control, motor control

Author Summary

Ageing affects the human neuromusculoskeletal system, which consists of that is muscles, bones, joints, nerves, and associated tissues. Since the human body had physiological and functional redundancy, humans will adopt their movement to compensate for these initial losses. Adaptation strategies affect joint loading, stability, and may lead to structural underuse of specific muscles, which especially in older adults leads to an accelerated decline of the underused part of their muscular system. Early detection can mitigate development of permanent movement impairments, but clinicians and scientists do not yet understand the course of compensatory muscle recruitment, and it is unclear how much decline can be tolerated before movement limitations begin. In experimental studies it is not possible to identify the effects of specific intrinsic properties; we therefore developed a generic neuromusculoskeletal model that can realistically simulate the effect of age-related changes in the neuromuscular system on daily life activity. Since standing up is a key daily life movement, we have focused on this movement, specifically sit-to-walk. We formulated a planar neuromuscular model driven by muscle reflexes and used optimization to design realistic controllers. We validated the simulations against experimental data.

1. Introduction

Adults rise from a seated position approximately 60 times a day (1). The inability to perform this task (e.g. from a seat or toilet) is associated with falls, frailty and institutional living(2). As the human movement system has physiological and functional redundancy, movement limitations do not promptly arise at the onset of physical decline (3,4). This makes prediction of movement limitations more complex as it is unclear how much decline can be tolerated before movement limitations arise.

Humans adapt their movement strategies throughout the lifespan. Humans develop compensation strategies to deal with reductions in neuromusculoskeletal capacity, altered reinforcement schemes, and alterations in the sensory input (Fig. 3) (5). In a recent experiment (6), we found that variables related to stability are probably most important in how we adapt our standing up strategy as we age. However, variables that affect stability, like neural capacity (e.g. motor noise, sensor noise, reduced nerve conduction velocities), are difficult to capture and distinguish from other motor control parameters in experimental set-ups.

Neuromusculoskeletal models have the potential to shed light on the interconnectivity and interdependency of neuromuscular capacity and adaptation during stand up. Where experimental studies cannot focus on isolated variables of age-related decline as all factors are interconnected, models allow to select the variables that we would like to study in isolation. However, to get to this phase, we first need a model and controller that can realistically simulate how reduced capacity and altered movement objectives affect the standing up movement.

There are studies that have examined muscular motor control in sit-to-stand. Caruthers et al. (2016) (7) and Smith et al. (2020) (8) used an inverse musculoskeletal approach to examine the individual muscle contributions to the sit-to-stand transfer based on measured experimental data. To study

compensation strategies, we however need a model that can generate movements 'de novo', without prescribed kinematics. Bobbert et al. (2016) (9) developed a predictive planar muscle-actuated optimal control model and used direct collocation approach to determine whether successful STS strategies could be found after muscle weakness or with reduced tibiofemoral compression forces. Their controllers are time history stimulation signals and therefore did not include the organization of the neural system. Also, the feet were fixed symmetrically at a fixed distance from the COM, which restricts compensatory movement strategies. Conclusions on successful STS despite muscular weakness are therefore only valid for this particular setup.

Sensorial feedback control models are a promising approach to realistically simulate human movement based on the principles of the neural control system. Geyer and Herr (2010) (10) were pioneers to develop a robust gait controller with a limited set of proprioceptive feedback loops, and their approach has been used in multiple studies since (11–13). Munoz et al. (2022) (14) developed a planar sit-to-stand sensorial feedback controller. Their study has however limitations when it comes to realistic simulation of adaptation strategies in standing up. Asymmetry in muscular activation and kinematics is common in STS, especially in an elderly or patient population (7,15,16), but was neglected. Concerning the neural controller, they included proprioceptive muscle length feedback via monosynaptic paths and vestibular feedback, thereby neglecting possible antagonistic paths and proprioceptive feedback from force and velocity, which are present in the neural organization. Also, the transitions between their controller states were based on seemingly arbitrary kinematic thresholds.

The aim of our study was to develop and validate a neuromusculoskeletal model with generic reflex-based muscle control to simulate the sit-to-walk movement for various conditions (seat height, foot placement), reduced muscular capacity, reduced neural capacity, and altered movement objectives. The stand-up controller uses delayed proprioceptive feedback from muscle length, force, velocity, and upper-body orientation (vestibular feedback) and includes monosynaptic an antagonistic

feedback paths. The transitions between the states are not prescribed but included as optimization parameter. The simulations were compared to recorded kinematics, ground reaction forces (GRF), and muscle activation (sEMG) from young (18-35 year) and older (>65 year) adults. The simulation framework and model are available (17).

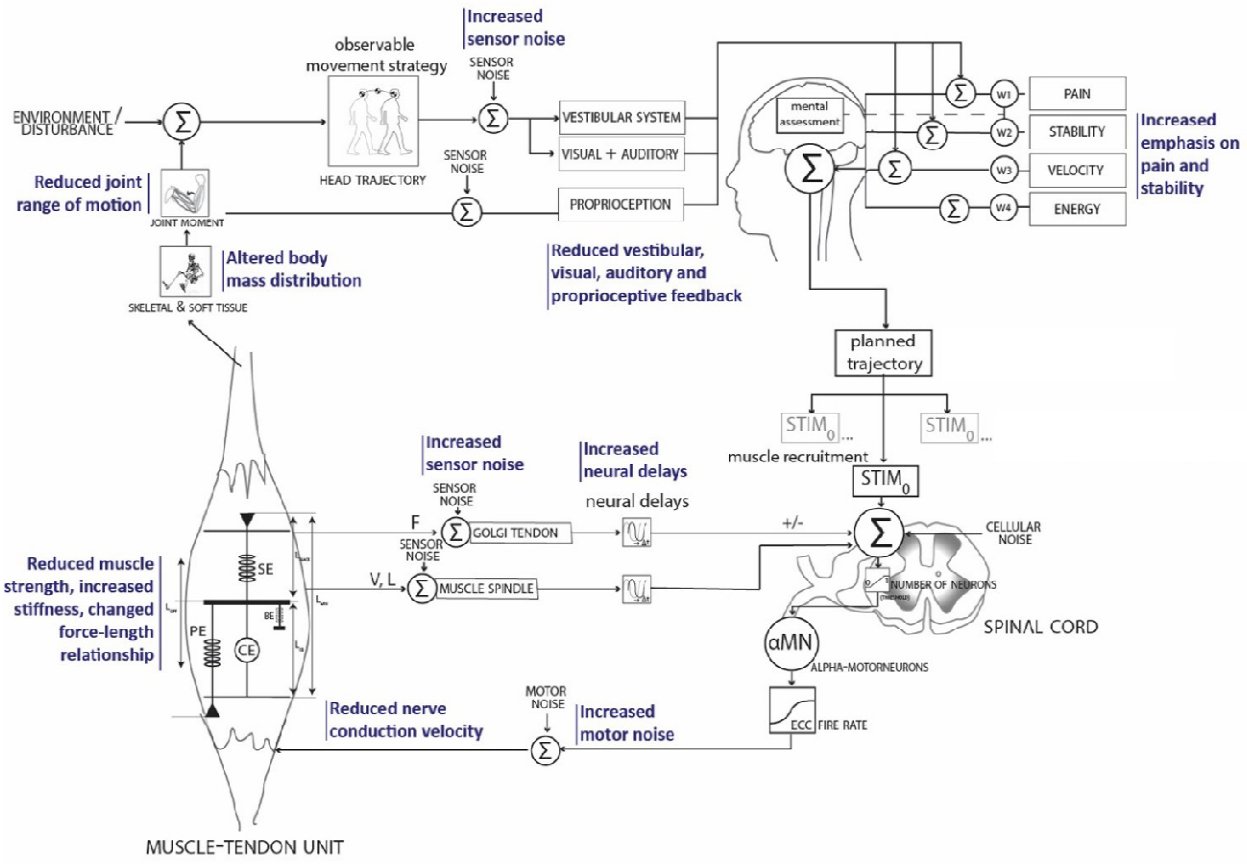

Figure 1 Feedback control of the neuromuscular system. In blue the parts of the neuromuscular system that start are known to have age-related changes (18).

2. Materials & Method

In summary, we developed a sit-to-walk musculoskeletal model and neuromuscular controller in which the control parameters were optimized using a shooting-based optimization method (19). The sit-to-walk controller consists of a two-phase stand-up controller (*P1, P2*) and a gait controller (*GAIT*) based on (10). The two-phase stand-up controller is based on proprioceptive feedback from muscle length, velocity, and force feedback, vestibular feedback and constant excitation (*C*), and uses separate feedback and excitation parameters for each phase. The feedback contains neural delays and includes both monosynaptic an antagonistic pathways. The free parameters were optimized to minimize the cubed muscle activation and gross cost of transport, at a prescribed minimum gait velocity, while avoiding falling, and excessive ligament stress. We ran multiple parallel optimizations with the same initial guess and used the best results as a starting point for the next round of optimizations. Final results were compared to a subset of recorded kinematics, ground reaction forces (GRF), and muscle activation (sEMG) from young (18-35 year) and older (>65 year) adults, in which participants were asked to stand up and walk to a table at self-selected speed (6). The simulations and optimizations were performed in SCONE (17) using the Hyfydy simulation engine (20).

2.1 Musculoskeletal model (H1120)

The musculoskeletal model (*H1120*) represents a male adult with a height of 1.80m and a mass of 75 kg optimized for predictive simulations (Fig. 2). The model has 11 degrees of freedom (dof): 3 dof joint between the pelvis and the ground, a pin joint (1-dof) at the hip and ankle, a 1-dof joint at the knee with coupled rotation and translation, a 1-dof lumbar joint, between the pelvis and the lumbar, and a 1-dof thoracic joint between the lumbar and the torso.

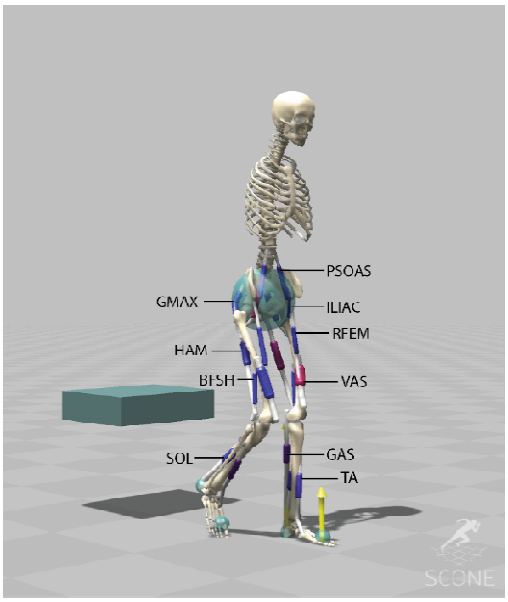

Figure 2 - The musculoskeletal model (H1120) has 11 degrees of freedom and is actuated using 20 Hill-type muscle-tendon units. The H1120 model is available on (17)*, comparison with existing opensource models is provided Supporting Files Table 1 and Supporting Files Figures 1-9.*

The model is actuated using 20 Hill-type muscle-tendon units (MTU) (21). This reduction in number of muscles was done by combining muscles with similar functions in the sagittal plane into single MTUs with combined peak isometric forces to represent 11 major bi-lateral muscle groups: gluteus maximus (GMAX), biarticular hamstrings (HAM), iliacus (ILIAC), psoas (PSOAS), rectus femoris (RF), vasti (VAS), Biceps Femoris short head (BFSH), gastrocnemius (GAS), soleus (SOL), tibialis anterior (TA).

Peak isometric forces were based on a lower limb model of Delp et al. (1990) (G2392) (22), peak force from this 43-MTU model were summed to obtain a model with reduced number of muscles (Supporting Files Table 1). The optimal fiber length and tendon slack length are based on G2392 (23) , except for HAM, BFSH, ILIACUS, PSOAS, where the updated model of Rajagopal et al. (2016) (RAJAG) was used (24). The model is free from wrapping surfaces, instead muscle paths were optimized using via-points to match the muscle moment arm data, peak normalized fiber length, and

normalized path lengths (muscle-tendon lengths – tendon slack length) from existing models and experimentally measured moment arms. The lumbar and thoracic joints are torque driven. The H1120 model is available on (17), comparison with existing opensource models (G2392 (23), G1018 (25), RAJAG (24), ARNOLD (26)) is provided in Supporting Files Table 1 and Supporting Files Figure 1-9.

2.1.1 H1120_STW

Contact forces between the feet and the ground and between the buttocks and the chair are modelled with Hunt Crossley force spheres and box respectively (27,28) (Fig. 2). Each foot has two contact spheres representing the heel and toes, each with a radius of 3 cm. The pelvis has one contact sphere of 12 cm representing the buttocks. The chair is represented as a box (40x12x5 cm). The contact spheres at the feet had a plane strain modulus of 17500 N/m .. cm^2 and at the chair 10000 N/m ...cm^2. All contact spheres have a dissipation coefficient of 1 s/m, static friction and dynamic friction coefficients of 0.9 and 0.6 respectively. Joint forces have a limit stiffness of 500 N/m, representing the ligaments.

2.1.2. Hyfydy model

The model is developed as an OpenSim 3 model and translated into a Hyfydy model to improve the simulation speed (20). Hyfydy is currently available as a plug-in for SCONE (19), which is Open Source Software for predictive simulations of biological motion. Both the OpenSim and Hyfydy version of the model are available.

2.2 Controllers

In the development of the sit-to-walk controller, we have tested several combinations of controllers, using muscle-reflex controllers and existing gait controllers (12). The most realistic and stable

controller was a combination of two reflex-controllers, which is in line with what other research groups found for the sit-to-stand movement (14), followed by gait control.

2.2.1 Standing up controller

The standing up controller is based on a reflex controller with two distinct states, each containing its own set of control parameters. The reflex controller is based on monosynaptic and antagonistic proprioceptive feedback from the muscles and vestibular feedback linked to the pelvis tilt (Table 1, Fig. 3a). The proprioceptive control is described by:

$$U = C_0 + K_L(L(t-\delta_t) - L_0 + K_F\big(F(t-\delta_t)\big) + K_V\big(V(t-\delta_t)\big) \quad (1)$$

In which K_L, K_F, K_V , the gains of the controller, and C_0, constant actuation, are optimized. , L_0, the length offset, is set to 1; although we could have optimized for this parameter, the result is a constant actuation ($K_L L_0$) hence the optimization would not have been able to distinct this from C_0. $L(t)$ is the normalized CE length ($L \quad /L_{opt}$) at time t. The torque driven lumbar and thoracic joints were controlled by a PD control and were dependent on the velocity and position of the respective joints.

Table 1 Neural latencies were implemented for the monosynaptic, antagonistic and vestibular controllers as multiples of 5ms. Compared to prior publications, HAM, BFSH, and RFEM have longer latencies (15ms instead of 10ms, 20ms instead of 10ms, and 20ms instead of 10ms respectively). Vestibular delays are higher compared to prior publications that used 20ms delays [ref Geyer & Herr].

Muscle	Monosynaptic control Δ_t (ms)	Antagonists	Antagonists control Δ_t (ms)	Vestibular control Δ_t (ms)
HAM	15	RFEM, VAS	20	45
BFSH	20	RFEM, VAS	20	45
GMAX	10	ILIAC, PSOAS	10	40
ILIAC	10	GMAX	10	40
PSOAS	10	GMAX	10	40
RFEM	20	HAM, BFSH	20	45
VAS	20	HAM, BFSH	20	45

GAS	35	TA	35	55
SOL	35	TA	35	55
TA	35	GAS, SOL	35	55
Lumbar				35
Thoracaic				30

Delays

Neural latencies were implemented for monosynaptic, antagonistic and vestibular feedback as multiples of 5ms due the range of the accuracy we could obtain for these parameters from literature. For the monosynaptic controllers for SOL the delay was set to 35 ms, based on the experimental measurements of the mean H-reflex latency (30.2ms, SD = 2.1), plus the distal motor latency (3.3ms, SD = 0.6ms) (15,29) . The latency of the reflex loop for GAS and TA were also set to 35 ms with the assumption of a similar length of reflex loop. RFEM latency was set to 20 ms, based on the patellar tendon reflex latencies (21ms, SD = 1.5 ms) (29) assuming the muscle spindle latency to be negligible (30). We assumed that VAS, and BFSH have a similar neural path length (31,32). We do expect the VAS and BFSH to have a slightly higher latency than the RFEM, but within the 5 ms margin. HAM has a lower latency and was set to 15 ms.

The other latencies were estimated based on the difference in motor distance between SOL and the particular muscle and the motor axon conduction velocity (CV) (about 50 m/s). We estimated the difference in motor distance between GMAX and SOL to be 50-60 cm, which resulted in 10ms latency for GMAX. We assumed PSOAS and ILIAC to have a similar path length as GMAX from the spinal cord. For the antagonistic controllers, we took the average of the delays of the two muscles involved.

The vestibular delay is based on electromyographic responses following galvanic vestibular stimulation (33). Note that large inter- and intra-subject differences have been reported on these responses (34). In general, the vestibular latency is a summation of latencies within the neural system, based on conduction velocity (CV) and the central nervous system (CNS) distance:

$$vestibular\ latency = \frac{motor\ distance}{motor\ axon\ CV} + \frac{CNS\ distance}{CNS\ CV} + central\ delay$$

We looked at the short latency responses. SOL has a mean vestibular short latency delay from stimulation to activation onset of 55ms (33,35). The latencies of the responses in TA are equivalent to those in SOL (35) and we assumed the GAS to have a similar response time. H-reflex latency plus the distal motor latency of SOL represent the time to travel the motor distance twice, plus the neuron delay in the spinal cord. With these values of SOL we could make a rough estimate for the other muscles on the vestibular latencies (Table 1):

$$MUSCLE_{vestibular-latency} = SOL_{vestibular-latency} - \frac{\Delta_{t-SOL}}{2} + \frac{\Delta_{t-MUSCLE}}{2}$$

The values were round down to integers of 5 ms. Results are in line with inter-muscular differences in medium latency delays reported in literature (34). For the lumbar joint we used $SOL_{vestibular-latency} - \frac{\Delta_{t-SOL}}{2}$ (35 ms). For the thoracic joint, we used an estimate of 30 ms based on the central delay and CNS CV estimates from (34).

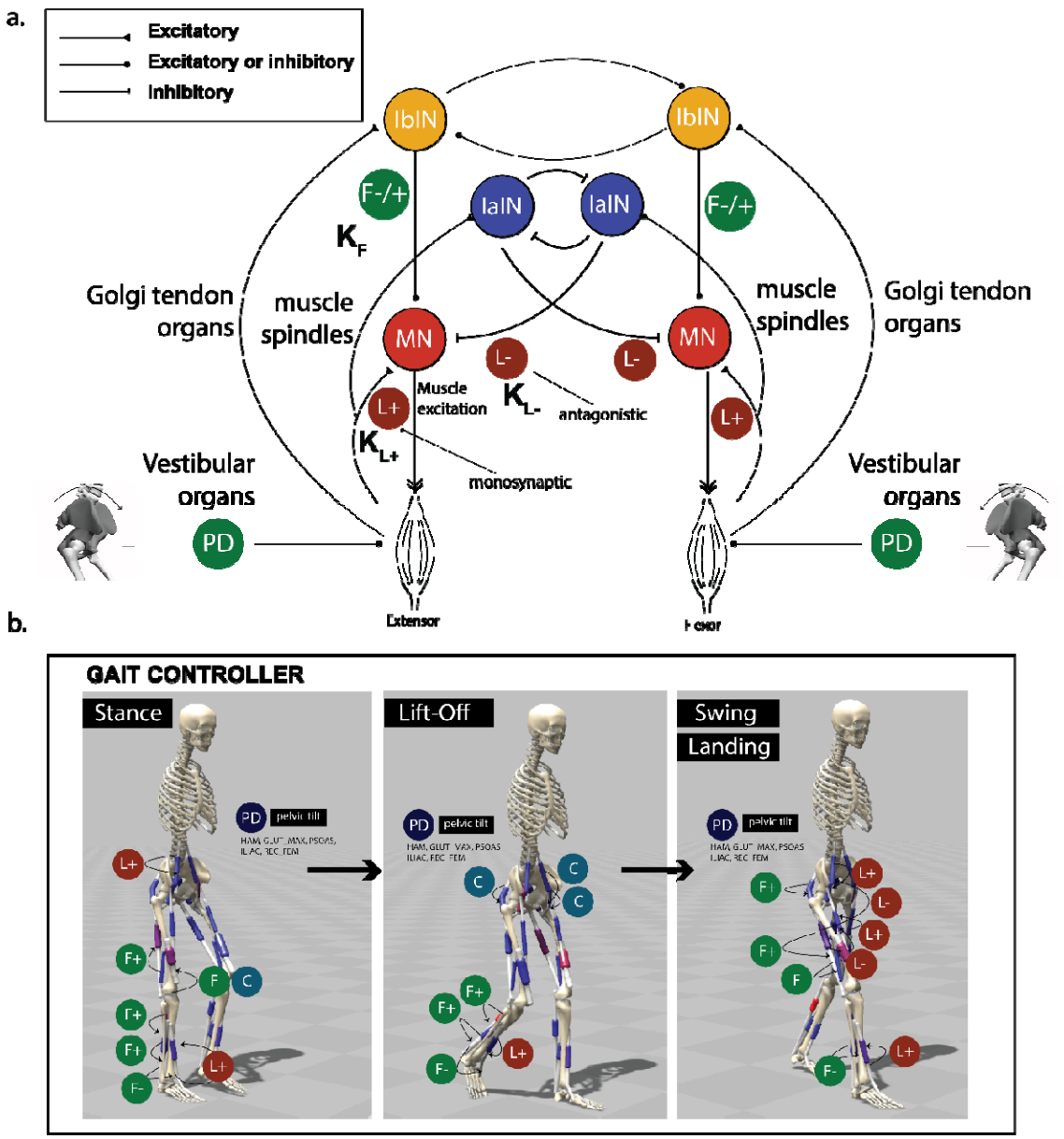

Figure 3 a) The reflex controller is based on proprioceptive and vestibular feedback for each muscle. Each muscle has a mono and/or antagonistic reflex control (Table 1). The standing up controller is based on two consecutive controllers (two states). b) The muscle-reflex gait controller is based on a previously published controller by Geyer & Herr (2010). We added the BFSH and RFEM controller to have both uni-articular muscles around the knee and bi-articular muscles surrounding the knee and hip, respectively. Additional we added controllers for the ILIAC and PSOAS muscles.

2.2.2 Gait controller

The muscle-reflex gait controller is based on a previously published controller by Geyer & Herr (2010) (10). The controller consists of 3 states: Stance (St), Lift-off (Lo) and Swing (Sw) outlined in Table 2 & Fig. 3. State transitions were determined by: 1) Lo to Sw: magnitude of ground reaction force (GRF) on the foot was lower than a threshold; 2) Sw to St: horizontal distance of the ipsilateral foot was behind the pelvis; 3) S to LO: magnitude of ground reaction force (GRF) on the ipsilateral foot was higher than a threshold. The GRF threshold was a parameter of the optimization process. We added the BFSH and RFEM to the Geyer & Herr (2010) controller to have both monoarticular muscles around the knee and bi-articular muscles surrounding the knee and hip, respectively. Both muscles are controlled through monosynaptic proprioceptive length and force feedback paths, with separate gains for each of the three states. For RFEM we added vestibular feedback control in Stance. We also had two additional hip flexors (ILIACUS and PSOAS) and two torque driven joints (thoracic and lumbar).We configured the ILIAC and PSOAS controllers like the HFL paths from Geyer & Herr. The torque driven lumbar and thoracic joints were controlled by a PD control (vestibular control) and were dependent on the velocity and position of the respective joints and independent of states. A PD controller was used to control the pelvis tilt angle (ϑ) and velocity (θ') with respect to ground, comparable to vestibular feedback, using the muscles crossing the hip joint (HAM, GMAX, ILIAC, PSOAS, RFEM) Note that the vestibular and neural latencies were updated to the values of Table 1 and therefore differ from previous models.

Table 2 Muscle feedback pathway of the length feedback (L), Force feedback (F), and constant (C). All monosynaptic muscle-based feedback laws were positive feedback laws for length (L+). All antagonistic muscle pair-based feedback laws (Anta) were negative feedback laws for length (L-)

Gait Controller

	Stance					Lift-off					Swing				
	VES	L	F	C	Anta	VES	L	F	C	Anta	VES	L	F	C	Anta
HAM															
BFSH					HAM(F)										HAM(F)
GMAX															
ILIAC															HAM(L)
PSOAS															
RFEM															HAM(L)
VAS			KA	KA											
GAS			*					*							
SOL			*					*							
TA		*			SOL(F) *		*			SOL(F)*		*			SOL(F)*

KA = knee angle
* = reflex gains do not modulate between states

2.2.3 Sit-to-walk controller

The sit-to-walk controller is a sequential controller consisting of the standing up controller (two-state reflex controllers) and a gait controller. The transition times between the reflex controllers and the gait controller were parameters of the optimization process.

States calculated from the model were muscle length (l), muscle velocity (v), muscle force (F), and pelvis tilt orientation (ϑ) and velocity (θ'). In total, there were 551 free parameters of the optimization, including the controller gains (K_C, K_{L+}, $K_{F\pm}$, K_p, and K_v), offsets for muscle length feedback (l_o), proportional feedback of ϑ (ϑ_o), proportional feedback of the lumbar and thoracic joints, transition times between the controllers, and stance load threshold for the gait state controller.

2.4 Simulation and optimization framework

The equation of motion and their integration was done in SCONE (19). The simulations started with different initial postures of the model's dof, while the velocities were set to 0. The selected initial positions were based on commonly used seating positions prior to stand-up (Fig. 4). The simulation

stopped when the maximum simulation time (12s) was reached or until the model fell, which was defined as the COM height being below 0.6 times of its height at the start of the simulation.

The optimization objective was to minimize the weighted sum of a set of measure terms, each of contributing to a high-level description of the sit-to-walk task.

Mimic measure: To save simulation time and increase optimization performance, a measure was used that defines how well the simulation mimics measured COM pelvis position (x, y). The purpose of this measure was to have a rough standing up trajectory for the model to start from without dictating any specific motion pattern; This measure becomes zero once the motion is roughly withing the boundary of the trajectory.

Gait velocity measure: This measure computed the average forward velocity of the model, and was used to promote locomotion at a predefined minimum velocity of 0.8 m/s. The value is normalized by the set minimum velocity. To allow the model time to reach the minimum velocity after standing up, the first three steps were not considered in the gait velocity evaluation. This measure becomes zero once the minimum velocity criterion is met.

Range measure: These measures penalize excessive joint limit forces and range of motion from ligaments, soft tissue, and joint geometry that are not present in the simplified model: lumbar extension (-50…0 degrees), thorax extension (-15…15 degrees), pelvis tilt (-50…30), ankle angle (-60…60). For the knee, there was a penalty on the DOF limit force (500 N/m) was out of range. All range measures become zero once within range or below their given thresholds.

Minimization of head acceleration: if no minimization for the head acceleration was set, simulation would produce a large initial peak in the ground reaction forces in gait. To represent how humans stabilize their vestibular and visual systems during gait, we added a head acceleration penalty with a

threshold of 1m/s^2 . This penalty measure returned to zero once the head acceleration is below the threshold.

Energy objective: Finally, an energy estimate was used as to minimize energy consumption during stand-up and minimize cost-of-transport during gait. The measure consisted of metabolic energy expenditure based on based on (36), complemented by minimized cubed muscle activations, and lumbar and thoracic joint torque minimization as substitute for the lack of trunk muscles. During the optimization, this measure eventually became the only non-zero term in the objective function.

2.4.1 Optimization algorithm

Optimization was performed using the Covariance Matrix Adaptation Evolutionary Strategy (CMA-ES) in the Open Source software SCONE (19). The population size of each generation was 10, the number of iterations was dependent on the simulation time. In line with previous studies (13), we have run multiple parallel optimizations with the same initial guess and used the best set as start the next set of optimizations.

2.5 Altered conditions, neuromuscular capacity, and movement objectives.

One of the applications for the controller is to determine how different seats or initial postures affect the sit-to-walk biomechanics and adaptation strategies. As an example we used the controller to learn STW from a lower seat (height = 35cm) (Fig. 4a), and when the feet were placed asymmetrically (anterior-posterior position) (Fig. 4b). We tested several other initial postures which are available (17).

2.6 Experimental data

To validate the simulations, we adopted a subset of kinematic and kinetic data from van der Kruk et al. (2022) (6), where kinematic and kinetic data of sit-to-walk at self-selected speed was recorded of

young (27.2±4.6 years, N = 27, 14♀) and older (75.9±6.3 years, N = 23, 12♀) adults. This study received ethical approval by the institutional ethics committee of Imperial College London, UK. All participants gave written informed consent. Participants were seated on an instrumented chair with armrests, which was adjusted in height to have an approximate 90^0 knee angle while seated in neutral position. The sit-to-walk movement was performed at self-selected pace and as-fast-as-possible each with 5 repetitions. The initial posture of the participants was not restricted (e.g. foot position, trunk angle, position on the seat), and participants were allowed to use their arms. For the verification purposes, only the trials of young participants that naturally stood up without arms were selected (45 trials). Note that the arms were not crossed on the chest, so arm swing was still allowed. Reaction forces were measured via two Kistler forceplates embedded in the walkway and one at the seat, and two 9129 AA Kistler forceplates in the armrests. A Vicon system with 10 cameras (MX T20) captured the STW volume (100 Hz). Participants were equipped with 84 reflective markers. A wireless Delsys EMG system with 16 sensors measured the EMG signal of specific muscle groups. The European guidelines for the EMG sensor placement were followed.

Marker trajectories and GRFs were translated into joint kinematics (inverse kinematics) and muscle forces (static optimisation) in OpenSim 4.2 using the musculoskeletal model of Rajagopal et al. (2016) (24). To compare muscle activations, a weighted sum of the muscle activations from the grouped muscles was calculated. Activations were weighted by the maximum isometric force of individual muscles divided by the total isometric force of the grouped muscles.

Muscle activation levels were compared to measured sEMG data for seven bi-lateral muscles (HAM, GMAX, RFEM, VAS, GAS, TA). Muscle excitations were determined from sEMG data that were high-pass filtered (30Hz), then full-wave-rectified, and low-pass filtered (6Hz) with zero-lag fourth order Butterworth filters. Since no Maximum Voluntary Contraction was available in the dataset, the excitation was normalized by the maximum excitation measured within the individual complete sit-

to-walk trials (stand up- walk 3 meter –turn – walk 3m – sit down). Note that as a result the activation levels indicated by the sEMG might be higher than the actual activation levels.

Simulations were verified by comparing joint angles, ground reaction forces, and muscle activations.

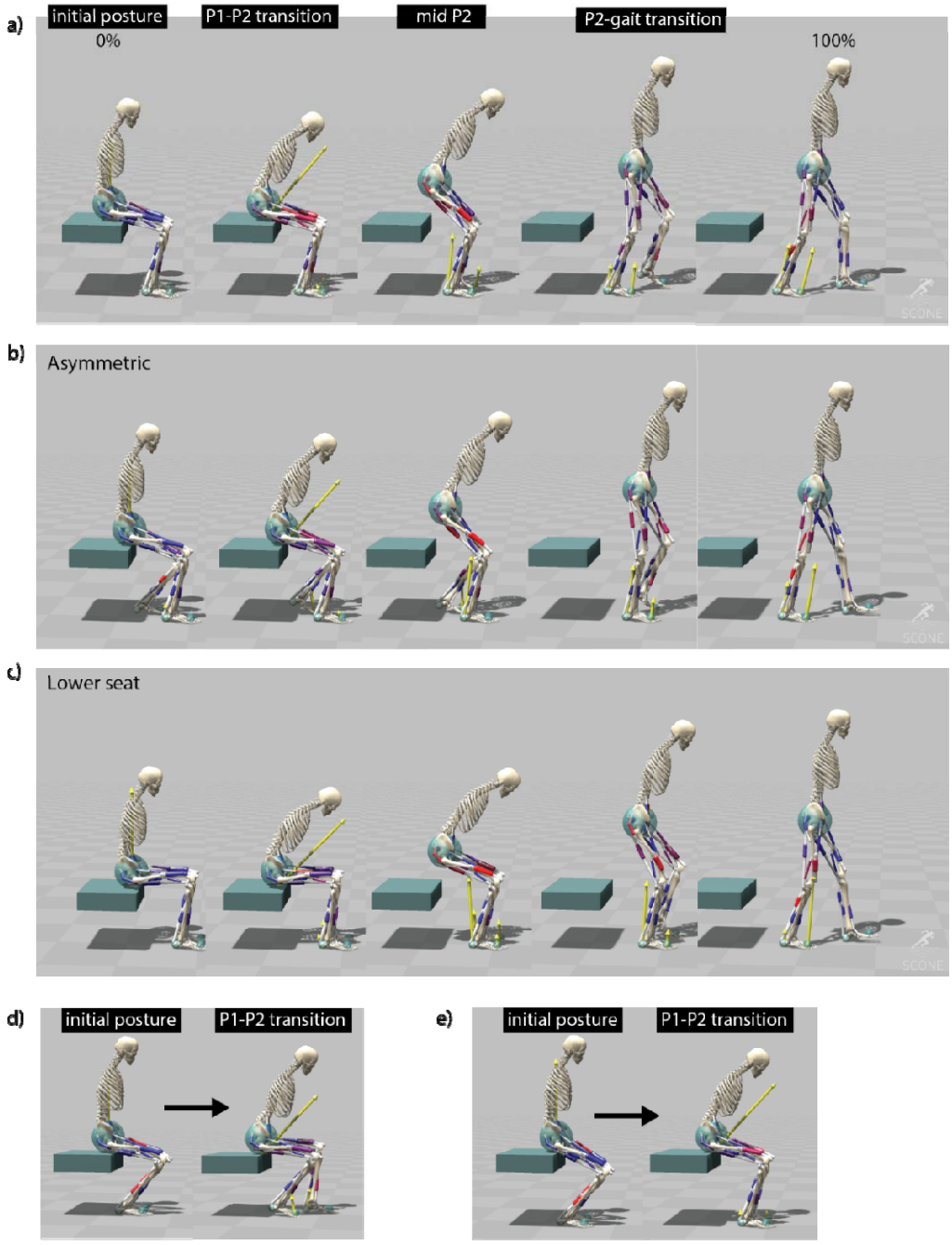

Figure 4 Sit-to-walk simulations; a) simulation with normal seat (seat height 44cm). Shown are the postures at t = 0, at the transition between the reflex controllers (P1-P2), midway P2, and at the transition from P2 to gait control; b) simulation where the initial posture of the model is an asymmetric position in the anterior-posterior direction; c) simulation with a lower seat height (35 cm); d,e) initial posture and posture at end of the first controller for a lower seat (d) and a higher seat (e). The initial feet positioning of the model was set backwards. The model uses P1 to reposition the feet to a better starting position for sit-to-stand transitioning.

3. Results

3.1 Sit-to-walk controller (normal posture)

The sit-to-walk simulation consists of three phases (P1,P2, GAIT). During P1, the model repositions the trunk, bending it forward (Fig. 4a). This repositioning has been extensively reported in experimental research(16,37) , and is in line with the measured kinematics (Fig. 5). We noted that when we changed the initial posture of the feet to a far backwards position, the P1 controller repositioned also the feet, placing them symmetrically or asymmetrically forward (Fig. 4 d,e). This is beneficial for the transition of the movement into the standing up and gait phase.

In P2, the model is extending from a seated position into the GAIT controller, transitioning into gait before the joints are fully extended (Fig. 4a). This is in line with human movement control in sit-to-walk (5) and reflected by the close resemblance of the measured knee and hip angles (Fig. 5). The higher knee and hip flexion during the first step (80%) are due to the lack of pelvis rotation and needed to create ground clearance (Fig. 5e).

Since no Maximum Voluntary Contraction was available in the dataset, the excitation was normalized by the maximum excitation measured within the individual complete sit-to-walk trials; as a result, sEMG activation data might be overestimated, and the focus was on the time of activation and the shape of the activation curve rather than the absolute difference in activation level. We found the simulated muscle activation timing to closely resemble the sEMG data (Fig. 6). VAS shows a close to maximum activation, which has to do with the relatively weak VAS muscle in the H1120 model. When comparing the simulated muscle forces to the muscle forces obtained via the static optimization (RAJAG model (24)), the forces are comparable (Fig. 6c). As a result of the simplified contact geometries of the chair and buttocks, there are differences in the ground and seat reaction forces. The course of the seat reaction forces is less fluent in the simulation. The ankle dorsiflexion, knee flexion, and hip flexion have a flatter course in P1 compared to measured kinematics. HAM is activated later and the HAM activation is earlier compared to measured sEMG (Fig. 6). The peak

simulated joint loading provides a reliable estimate for all joints, except for the ankle joint of the stance leg during the first step. Here the predictive simulation underestimates the ankle joint loading (Fig. 7).

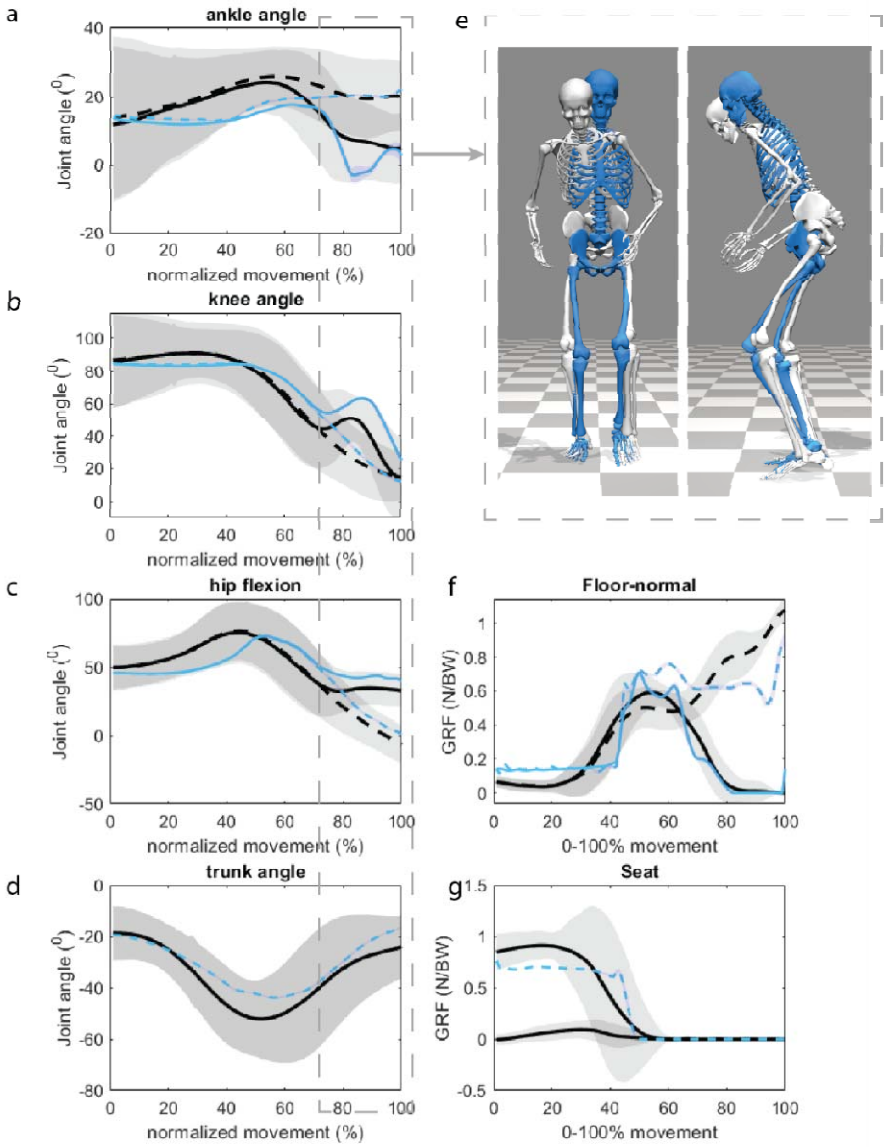

Figure 5: measured and simulated joint kinematics and reaction forces.

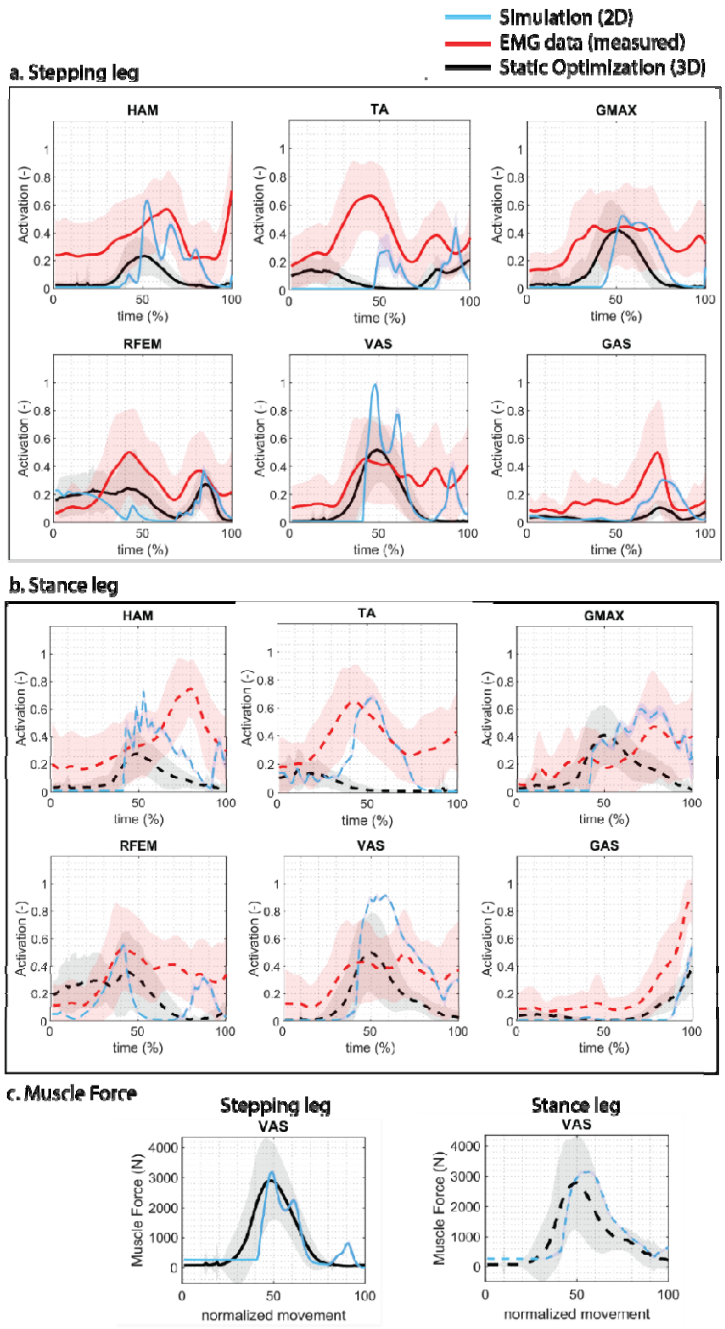

Figure 6: Muscle Activations. In red, the mean measured EMG data of # trials. Measured EMG data is normalized to the peak signal measured within the complete STW trial for each trial per participant, since no data on maximum voluntary contraction was available. Therefore, the normalized EMG data can be overestimated. In black, the mean muscle activations obtained from the inverse dynamics approach with static optimization of a 3D musculoskeletal model and measured kinetics; shade indicates +/- one standard deviation. In green, the muscle activations from the predictive simulation with the 2D controller and model.

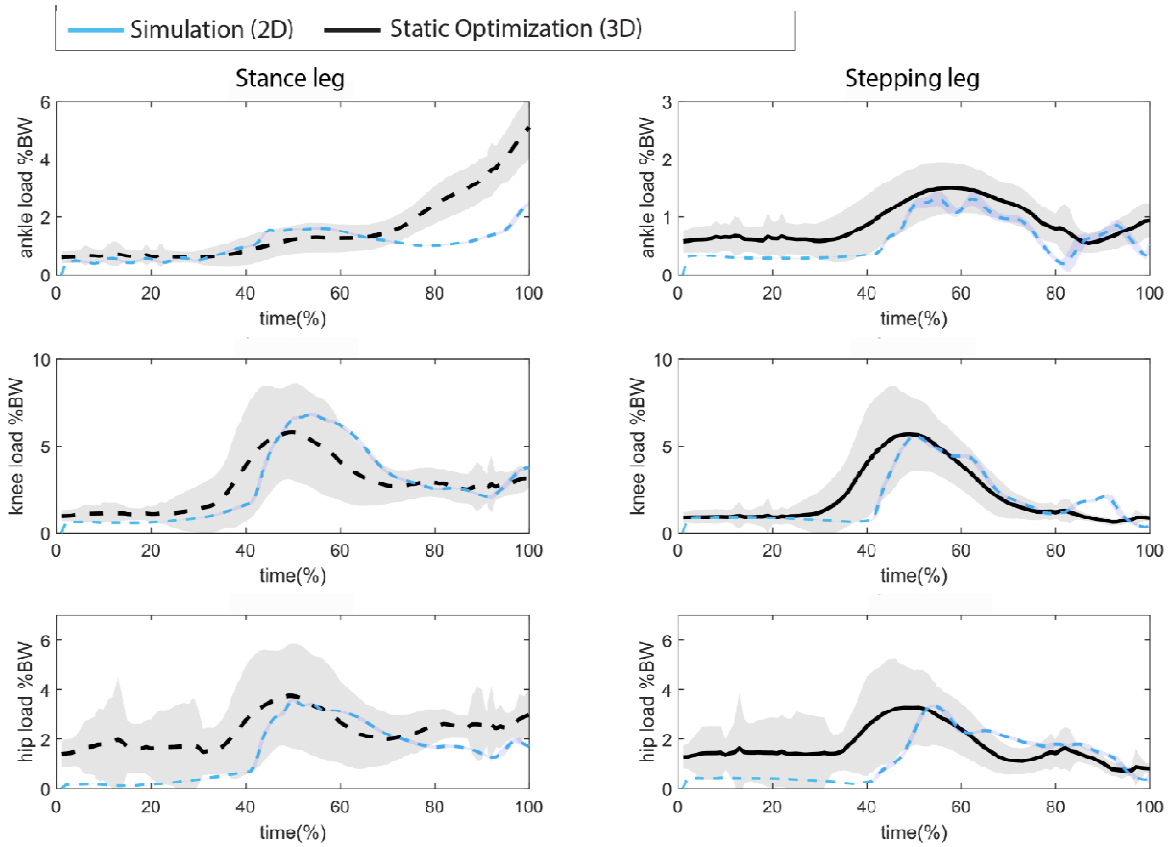

Figure 7 : Knee joint load comparison between measured knee load estimation (inverse kinematics, static optimization, 3D musculoskeletal model (RAJAG)) and the simulated knee joint loading. The load is comparable.

3.2 Alternative Conditions

3.2.1 Lower seat

When the height of the seat was reduced, the model showed a larger trunk angle in P1, which is in line with human motor control (5) (Fig. 4c). As expected, the lower seat requires higher muscle activations and results in greater joint loads (Fig. 8). The lower seat results in higher peak joint loadings compared to the normal seat: knee load +15 and +21%, ankle load +21% and +51%, hip +9% and +10% for the step and stance leg respectively. The biggest differences in muscle activation is an

increased activation of the BFSH, TA, and PSOAS in the rising phase of the stepping leg, and the GMAX in the rising phase of the stance leg.

3.2.2 Asymmetric feet

During asymmetric foot positioning, the trunk was kept more upright than during symmetric conditions (Fig. 4b). This posture results in a large reduction of hip load in stepping leg compared to the normal condition (-24%) (Fig. 8). The bilateral knee loads are also slightly reduced (-1-3%), whereas the ankle load in stepping leg is higher compared to the normal condition (+71%) at the initiation of the movement. There is less activation for HAM in in the stepping leg, whereas RFEM and GAS are more activated (higher peak and duration) compared to the symmetric feet position in the stepping leg. In summary, an asymmetric foot positioning in which the stepping leg is placed backwards, leads to a large reduction of peak hip load in the stepping leg with the drawback of increased peak ankle load in the stepping leg.

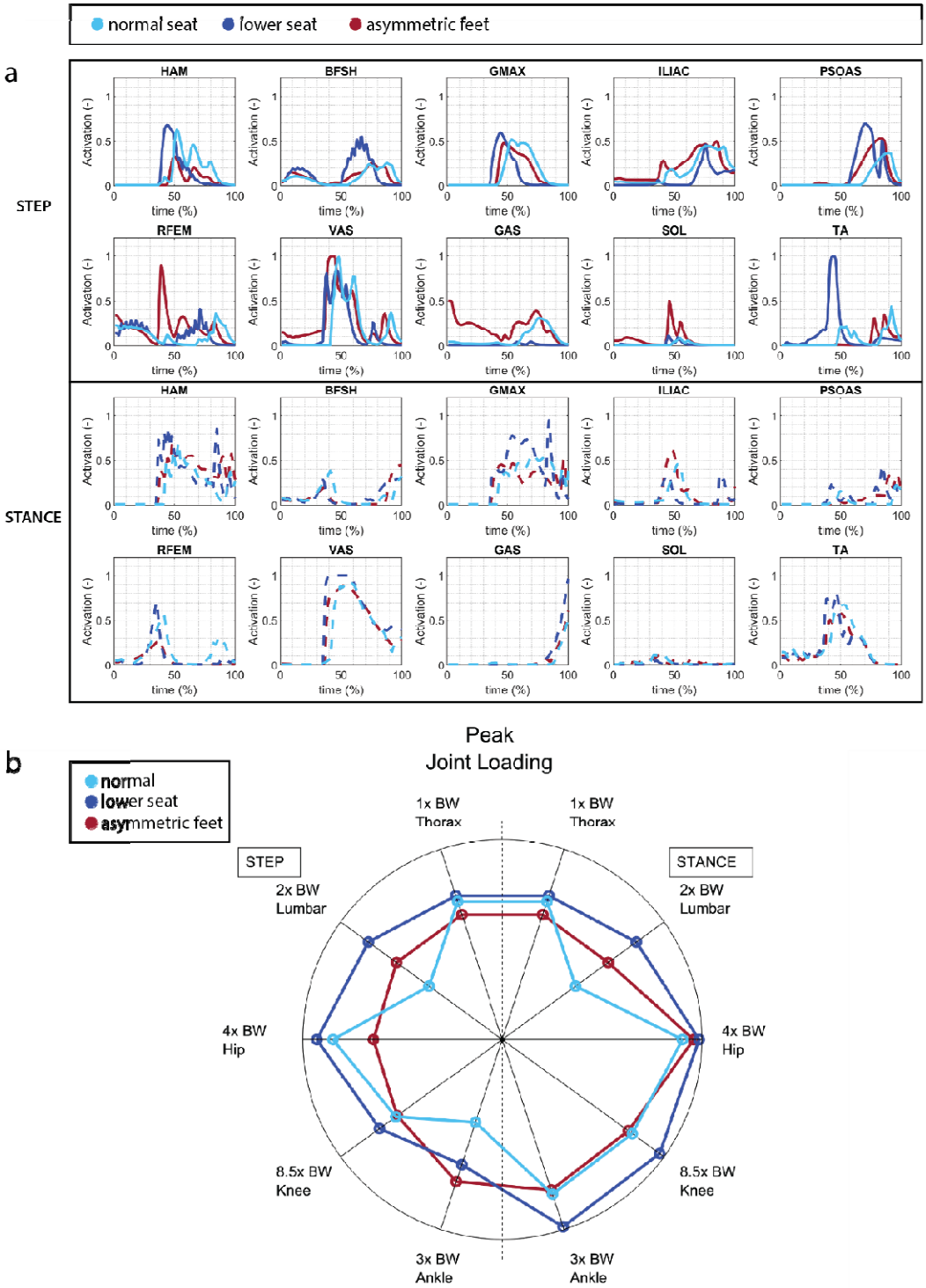

Figure 8 a) Muscle activation for lowered seat and asymmetric foot positioning. the lower seat requires higher muscle activations than the normal seat condition. B) peak joint loading for alternative seat height and foot positioning. Note that the thoracic and lumbar joints are torque actuated joints, so the load resulting from muscle force contraction is missing in these joints. The lower seat condition results in higher joint loads. The asymmetric foot positioning in which the stepping leg is placed backwards, leads to a large reduction of peak hip load in the stepping leg with the drawback of increased peak ankle load in the stepping leg.

460 **4. Discussion**

461 Progression of neuromuscular decline can lead to incorrect or insufficient compensation strategies
462 (maldaptation), both through altered muscle recruitment and changes in movement trajectories.
463 Predictive neuromuscular simulations are an effective tool for discovering those strategies, enabling
464 clinicians to design treatments that are both more effective and efficient for prolonging the mobility
465 of the patient. In this study we have developed a planar predictive neuromuscular simulation of the
466 sit-to-walk movement based on reflex controllers. The parts of the neuromuscular system and
467 altered movement priorities that are prone to age-related decline (Fig. 1) are part of the framework,
468 which therefore enables studies on how age-related changes affect sit-to-walk movement strategies.
469 The predictive planar lower limb model produced sit-to-walk movements that match real-world
470 kinematic and kinetic recordings. We demonstrated that the model can adapt to produce realistic
471 compensation strategies, by simply changing conditions such as seat height and initial foot
472 positioning.

473

474 We found that a 2-phase reflex based neural controller can realistically simulate the task of standing
475 up (38), which is in line with Munoz et al. (2022) (14) planar sit-to-stand simulation, and is different
476 from the commonly reported 4-phase kinematic phases (37). In our model, the transition time is
477 part of the optimization. The model is sensitive to this timing, especially when the conditions like
478 seat height are changed, which requires a quick re-optimization of the transition times for new
479 conditions. Prescribing the transition as a kinematic parameter would ignore the fact that the
480 adaptation of reflex gains occurs before a change in kinematics. We therefore believe it is important
481 keep this parameter independent.

482

483 Our planar sit-to-walk framework allows for asymmetric strategies, like asymmetric foot positioning,
484 and asymmetries in muscular capacities. Previous studies on sit-to-stand simulation did not allow for
485 asymmetry (9,14) which limits the available compensation strategies, and may not properly reflect

486 daily life movements as a result (16). Asymmetric strategies in standing up may have potential
487 implications for long-term joint degeneration due to altered joint loading and provide valuable
488 insights for clinicians in advising patients on the best strategy to avoid over- or unloading after
489 surgery or injury. The simulations show that an asymmetric foot positioning leads to a large
490 reduction of unilateral peak hip load with the drawback of increased peak ankle load.

491 Regarding the musculoskeletal model, the maximum isometric forces are based on (23) in which VAS
492 muscles are relatively weak for a healthy adult, as shown by the maximum activation of this muscle
493 while rising from the chair. When using the simulations for comparison of changes in muscular
494 capacity, the musculoskeletal model would benefit from other estimates of the maximum isometric
495 forces for young and older adults. With respect to the foot contact model, previous studies have
496 shown the importance of choice in foot models and foot stiffness for 3D predictive simulations (39).
497 However, for our planar model we found that the simulation produced consistent results over wide
498 ranges of stiffness settings.

499 **4.3 Limitations simplified model**

500 The simplified model and controller cause several simulation artefacts, which researchers and
501 clinicians should be aware of during interpretation.

502 - In sit-to-walk humans use medial-lateral trunk and pelvis movements for balance and foot-
503 ground clearance. This cannot be captured by a planar model.
504 - The buttocks are modelled by a single sphere. In reality, the contact with the chair is much
505 longer as the thighs roll off over the chair. This simplified contact geometry of the contact
506 spheres results in a flatter course of the ankle dorsiflexion, knee flexion and hip flexion prior
507 to seat off.
508 - Optimizations within the framework can result in different movement strategies starting
509 from the same scenario. For this manuscript we chose to select the strategy in which the
510 cost was lowest. However, there were movement strategies with a cost very close to the

minimal cost function with different yet equally realistic strategies. In future studies, we might want to treat these simulations as intra-trial differences of participants and report the distribution in kinematics and kinetics, as we would do with experimental data. This also makes the results less sensitivity to the cost function.

- Finally, our experimental study showed that >80% of the older adults used their arms to push off while standing up in a daily life setting (6). These compensatory strategies were not captured by this model. For example, (40) found that Osteoarthritis patients employ asymmetric arm strategies, possibly to unload the knee. Adding torque or muscle driven arms to the model would allow to determine whether this strategy is to compensate for a loss in muscular capacity or for pain unloading. Also, the use of the contralateral arm, e.g. by pushing on the knee, would generate insight into the aim of this strategy: stability or transferring the load over the joints (6).

4.4 Future work

The treatment of age-related mobility impairments is increasingly relevant in our ageing societies. These impairments typically do not arise at the onset of age-related physical decline, due to the physiological and functional redundancy of the human movement system. Predictive models that generate kinematics de novo have the potential to simulate the capacity versus compensation relationship, since they can generate new movement trajectories. This framework is now publicly available to test hypotheses on the sit-to-walk movement, answer 'what if' questions, or employ in design processes.

Data Availability statement

The source code and data for the predictive framework and the results presented in this manuscript are available from Git repository: (17)

Financial Disclosure Statement

This study was funded by NWO-TTW VENI Grant 18145(2021). The funders had no role in study design, data collection and analysis, decision to publish, or preparation of the manuscript.

References

1. Dall PM, Kerr A. Frequency of the sit to stand task: an observational study of free-living adults. Appl Ergon. 2010;41(1):58–61.
2. Fuller GF. Falls in the elderly. Am Fam Physician. 2000;61(7):2159–68.
3. Lipsitz LA. Dynamics of stability: the physiologic basis of functional health and frailty. J Gerontol A Biol Sci Med Sci. 2002;57(3):B115–25.
4. van der Kruk E, Silverman AK, Koizia L, Reilly P, Fertleman M, Bull AMJ. Age-related compensation: Neuromusculoskeletal capacity, reserve & movement objectives. J Biomech. 2021;122:110385.
5. van der Kruk E, Silverman AK, Reilly P, Bull AMJ. Compensation due to age-related decline in sit-to-stand and sit-to-walk. J Biomech. 2021;110411.
6. van der Kruk E, Strutton P, Koizia LJ, Fertleman M, Reilly P, Bull AMJ. Why do older adults stand-up differently to young adults?: investigation of compensatory movement strategies in sit-to-walk. npj Aging. 2022;8(1):1–19.
7. Caruthers EJ, Schneider G, Schmitt LC, Chaudhari AMW, Siston RA. What are the effects of simulated muscle weakness on the sit-to-stand transfer? Comput Methods Biomech Biomed Engin. 2020;23(11):765–72.
8. Smith SHL, Reilly P, Bull AMJ. A musculoskeletal modelling approach to explain sit-to-stand difficulties in older people due to changes in muscle recruitment and movement strategies. J Biomech. 2020;98:109451.
9. Bobbert MF, Kistemaker DA, Vaz MA, Ackermann M. Searching for strategies to reduce the mechanical demands of the sit-to-stand task with a muscle-actuated optimal control model. Clinical Biomechanics. 2016;37:83–90.
10. Geyer H, Herr H. A muscle-reflex model that encodes principles of legged mechanics produces human walking dynamics and muscle activities. IEEE Transactions on neural systems and rehabilitation engineering. 2010;18(3):263–73.
11. Song S, Geyer H. Predictive neuromechanical simulations indicate why walking performance declines with ageing. J Physiol. 2018;596(7):1199–210.
12. Waterval NFJ, Veerkamp K, Geijtenbeek T, Harlaar J, Nollet F, Brehm MA, et al. Validation of forward simulations to predict the effects of bilateral plantarflexor weakness on gait. Gait Posture. 2021;87:33–42.

13. Ong CF, Geijtenbeek T, Hicks JL, Delp SL. Predicting gait adaptations due to ankle plantarflexor muscle weakness and contracture using physics-based musculoskeletal simulations. PLoS Comput Biol. 2019;15(10):e1006993.

14. Muñoz D, De Marchis C, Gizzi L, Severini G. Predictive simulation of sit-to-stand based on reflexive-controllers. PLoS One. 2022;17(12):e0279300.

15. van der Kruk E, Strutton P, Koizia LJ, Fertleman M, Reilly P, Bull AMJ. Why do older adults stand-up differently to young adults?: investigation of compensatory movement strategies in sit-to-walk. npj Aging. 2022;8(1):13.

16. van Der Kruk E, Silverman AK, Reilly P, Bull AMJ. Compensation due to age-related decline in sit-to-stand and sit-to-walk. J Biomech. 2021;122:110411.

17. van der Kruk E, Geijtenbeek T. Repository sit-to-walk simulations. https://github.com/BODIES-Lab-TU-Delft/Sit-to-walk-predictive-simulations. 2023.

18. van der Kruk E, Silverman AK, Koizia L, Reilly P, Fertleman M, Bull AMJ. Age-related compensation: Neuromusculoskeletal capacity, reserve & movement objectives. J Biomech. 2021;122:110385.

19. Geijtenbeek T. Scone: Open source software for predictive simulation of biological motion. J Open Source Softw. 2019;4(38):1421.

20. Geijtenbeek T. https://hyfydy.com/. HyfyDy.

21. Millard M, Uchida T, Seth A, Delp SL. Flexing computational muscle: modeling and simulation of musculotendon dynamics. J Biomech Eng. 2013;135(2).

22. Delp SL, Loan JP, Hoy MG, Zajac FE, Topp EL, Rosen JM. An interactive graphics-based model of the lower extremity to study orthopaedic surgical procedures. IEEE Trans Biomed Eng. 1990;37(8):757–67.

23. Delp SL, Loan JP, Hoy MG, Zajac FE, Topp EL, Rosen JM. An interactive graphics-based model of the lower extremity to study orthopaedic surgical procedures. IEEE Trans Biomed Eng. 1990;37(8):757–67.

24. Rajagopal A, Dembia CL, DeMers MS, Delp DD, Hicks JL, Delp SL. Full-body musculoskeletal model for muscle-driven simulation of human gait. IEEE Trans Biomed Eng. 2016;63(10):2068–79.

25. Seth A, Thelen D, Anderson F, Scott D. https://github.com/opensim-org/opensim-models/tree/master/Models/Gait10dof18musc. Gait10dof18musc.

26. Arnold EM, Ward SR, Lieber RL, Delp SL. A model of the lower limb for analysis of human movement. Ann Biomed Eng. 2010;38:269–79.

27. Hunt KH, Crossley FRE. Coefficient of restitution interpreted as damping in vibroimpact. 1975;

28. Hertz H. On the contact of elastic solids. Z Reine Angew Mathematik. 1881;92:156–71.

29. Frijns CJM, Laman DM, Van Duijn MAJ, Van Duijn H. Normal values of patellar and ankle tendon reflex latencies. Clin Neurol Neurosurg. 1997;99(1):31–6.

30. Schäfer SS, Schuppan O, Dadfar F. The response of muscle spindle primary afferents to simultaneously presented sinusoidal and ramp-and-hold stretches. Brain Res. 1999;819(1–2):89–107.

31. Voight ML, Wieder DL. Comparative reflex response times of vastus medialis obliquus and vastus lateralis in normal subjects and subjects with extensor mechanism dysfunction: an electromyographic study. Am J Sports Med. 1991;19(2):131–7.

32. Palmieri RM, Ingersoll CD, Hoffman MA. The Hoffmann reflex: methodologic considerations and applications for use in sports medicine and athletic training research. J Athl Train. 2004;39(3):268.

33. Britton TC, Day BL, Brown P, Rothwell JC, Thompson PD, Marsden CD. Postural electromyographic responses in the arm and leg following galvanic vestibular stimulation in man. Exp Brain Res. 1993;94:143–51.

34. Ali AS, Rowen KA, Iles JF. Vestibular actions on back and lower limb muscles during postural tasks in man. J Physiol. 2003;546(2):615–24.

35. Fitzpatrick R, Burke D, Gandevia SC. Task-dependent reflex responses and movement illusions evoked by galvanic vestibular stimulation in standing humans. J Physiol. 1994;478(2):363–72.

36. Wang JM, Hamner SR, Delp SL, Koltun V. Optimizing locomotion controllers using biologically-based actuators and objectives. ACM Transactions on Graphics (TOG). 2012;31(4):1–11.

37. Schenkman M, Berger RA, Riley PO, Mann RW, Hodge WA. Whole-body movements during rising to standing from sitting. Phys Ther. 1990;70(10):638–48.

38. van der Kruk E, Geijtenbeek T. Predictive neuromuscular simulation of the sit-to-walk movement. In: International Society of Biomechanics. 2021.

39. D'Hondt L, De Groote F, Afschrift M. A dynamic foot model for predictive simulations of gait reveals causal relations between foot structure and whole body mechanics. bioRxiv. 2023;2023.

40. Komaris DS, Govind C, Murphy A, Ewen A, Riches P. Identification of movement strategies during the sit-to-walk movement in patients with knee osteoarthritis. J Appl Biomech. 2018;34(2):96–103.